# Structural Study of the Two Phases of Tetrakis(methylseleno)-tetrathiafulvalene ($TSeC_1$-TTF)

Chikako NAKANO,*,†† Ping WANG, Takehiko MORI, Yusei MARUYAMA, Hiroo INOKUCHI, Hideki YAMOCHI,† and Gunzi SAITO†

Institute for Molecular Science, Myodaiji, Okazaki 444

†Department of Chemistry, Faculty of Science, Kyoto University, Sakyo-ku, Kyoto 606

(Received March 20, 1991)

The crystal structure of the low-melting point phase (L-phase) of a single component organic semiconductor, $TSeC_1$-TTF, is determined and compared with that of the high-melting point phase (H-phase). The intracolumnar overlap mode and the calculated intermolecular overlap integrals are slightly larger in the L-phase, to which is ascribed the low resistivity of the L-phase. The L-phase, however, does not have two-dimensional networks of intercolumnar Se···Se contacts, which exist in the H-phase. This may be associated with the difference of the melting points.

Tetrakis(alkylthio)tetrathiafulvalenes($TTC_n$-TTFs) are very unique semiconductors with fairly low resistivity as single component organic compounds. This character is derived from the short intermolecular distance between the adjacent central $\pi$ systems, because a bundal of long alkyl chains assemble $TTC_n$-TTF molecules in a fashion that the central $\pi$-systems can pile up one after the other very tightly (Fastener Effect).[1,2] $TTeC_n$-TTFs and $TSeC_n$-TTFs, in which the outer sulfur atoms of $TTC_n$-TTF are replaced by Te and Se atoms respectively, were designed in order to increase the intermolecular interactions. We have found that $TTeC_1$-TTF reveals noticeably low resistivity of $8.1\times10^4$ ($\Omega$ cm) although alkyl chains are too short to attain the Fastener Effect.

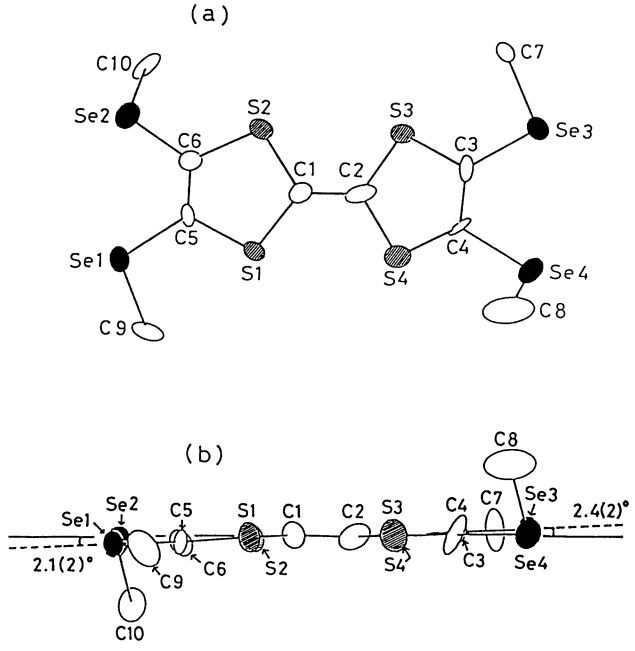


Fig. 1. The molecular structure of $TSeC_1$-TTF(L).
(a) The numbering scheme,
(b) Side view.

†† Toyota research fellow.

The $TTeC_1$-TTF crystal has very unique packing and intercolumnar zigzag Te···Te interactions along the stacking axis.[3] The title compound, $TSeC_1$-TTF, (Fig. 1) crystallizes in two phases, of which electrical conductivities are different by two orders.[4,5] We have reported the structure of the H-phase crystal, $TSeC_1$-TTF(H), in the previous paper.[6] In order to discuss the differences of electrical and thermal properties between these two phases, here, we report the structure of the L-phase crystal, $TSeC_1$-TTF(L) and compare the intermolecular overlap integrals with those of $TSeC_1$-TTF(H).

## Experimental

The synthesis of the $TSeC_1$-TTF compound was reported in the preceding paper.[4] Two kinds of single crystals were prepared by recrystallization from different solvents. Red needle crystals ($TSeC_1$-TTF(L)) were obtained from the mixture of hexane and benzene. On the other hand, dark red plate crystals ($TSeC_1$-TTF(H)) were obtained from pure hexane solution, sometimes together with red needle crystals.

Intensity data of X-ray diffraction were measured on a Rigaku automated four-circle X-ray diffractometer AFC-5R by the $\theta$-$2\theta$ scan technique with graphite monochromatized Mo $K\alpha$ radiation ($2\theta<60°$). Crystal data ($TSeC_1$-TTF(L)): $C_{10}H_{12}S_4Se_4$, F.W.=576.28, orthorhombic, space group $Pca2_1$, =18.534(5), $b$=5.284(1), $c$=17.533(4) Å, $V$=1717.0(7) Å$^3$, $Z$=4, $D_x$=2.23 g cm$^{-3}$ and $\mu$(Mo $K\alpha$)=89.12 cm$^{-3}$, crystal size: 0.02×0.6×0.04 mm$^3$. The intensity variation of the three standard reflections during the measurement was less than 5%. 2925 unique reflections were measured. The intensity data were corrected for absorption effects using a Gaussian integration procedure. The crystal structure was solved by the Patterson method and refined by the block-diagonal least squares procedure by using 1145 independent reflections ($|F_o|>3\sigma(|F_o|)$). The final $R$=0.072, $R_w$=0.068 $\{w=[\sigma^2+(0.015\,F_o)^2]^{-1}\}$ and $(\Delta/\sigma)_{max}$=0.89. Thermal parameters were anisotropic for all the non-hydrogen atoms and isotropic for hydrogen atoms. In the final difference Fourier map, the residual electron density corresponds to |1.7| e Å$^{-3}$ near Se1 atom. Although we assumed the space group was *Pcam* first, in this case we found difficulty in analyzing the structure.

The atomic scattering factors were taken from the International Tables for X-ray Crystallography.[7] All the calculations were carried out on a HITAC M-680H computer with the UNICS III program system.[8]

## Results and Discussion

Final atomic coordinates of $TSeC_1$–TTF(L) are shown in Table 1.[9] The molecule is noncentrosymmetric, while the $TSeC_1$–TTF(H) molecule is centrosymmetric,[6] and the terminal parts are slightly twisted because of the large atomic radius of Se atom as compared with those of the S and C atoms (Fig.1). The dihedral angles between the central $C_2S_4$ part and terminal $C_2S_2Se_2$ are 2.4(2)° and 2.1(2)°, respectively ($TSeC_1$–TTF(H): 2.72(5)°).

$TSeC_1$–TTF(L) molecules are stacked along the *b*-axis (corresponds to the needle axis) and the overlapping mode is shown in Fig. 2. Although the shortest intracolumnar S ··· S distance is a little longer than that of $TSeC_1$–TTF(H), the overlap along the stacking axis is a little larger. The shortest intracolumnar S ··· S distance is 3.73(1) Å and Se ··· S distances are 3.856(8) Å and 3.885(8) Å. There is no short Se ··· Se contact within a column in both two phases. The distance between the two least squares planes of the central

Table 1. Positional Parameters ($\times 10^4$) and Equivalent Isotropic Thermal Parameters of the $TSeC_1$–TTF (L)

$$B_{eq}=\frac{4}{3}(\sum_i\sum_j B_{ij}\boldsymbol{a}_i\boldsymbol{a}_j)$$

| Atom | *x* | *y* | *z* | $B_{eq}$/Å$^2$ |
|---|---|---|---|---|
| Se1 | 5599(2) | 9560(6) | 3372(2) | 2.9 |
| Se2 | 5085(2) | 7588(6) | 5188(2) | 3.9 |
| Se3 | 1902(2) | −4586(5) | 3030(2) | 2.8 |
| Se4 | 2431(2) | −2783(6) | 1239(2) | 3.8 |
| S1 | 4483(4) | 5445(15) | 2825(4) | 2.6 |
| S2 | 4065(4) | 3735(14) | 4363(4) | 2.8 |
| S3 | 3023(4) | −476(15) | 3626(4) | 3.0 |
| S4 | 3420(5) | 1194(15) | 2071(4) | 3.5 |
| C1 | 3945(14) | 3418(50) | 3355(14) | 2.5 |
| C2 | 3517(16) | 1533(50) | 3052(14) | 3.0 |
| C3 | 2599(14) | −1920(43) | 2858(14) | 2.2 |
| C4 | 2852(18) | −1106(49) | 2147(14) | 3.7 |
| C5 | 4926(13) | 6931(43) | 3603(14) | 2.0 |
| C6 | 4751(14) | 6154(52) | 4294(14) | 2.5 |
| C7 | 1933(18) | −4517(57) | 4170(14) | 4.0 |
| C8 | 2019(22) | 371(76) | 821(18) | 6.5 |
| C9 | 5646(16) | 9420(65) | 2301(16) | 4.1 |
| C10 | 5424(18) | 4588(60) | 5739(15) | 3.9 |

Table 2. Differences between the Two Phases of $TSeC_1$–TTF

| Phase | L | H |
|---|---|---|
| Solvent | Hexane and benzene | Hexane |
| Color | Red | Dark red |
| Crystal shape | Needle | Plate |
| Melting point/ °C[4] | 92.5 | 106.3 |
| Electrical resistivity along the stacking axis/Ω cm[4] | $1.0\times10^6$ | $2.7\times10^8$ |
| Activation energy/eV[4] | 0.26 | 0.58 |
| Density/g cm$^{-3}$[6] | 2.23 | 2.22 |
| Distance between the least square planes/Å | 3.568(4) | 3.570(1) |
| The shortest intracolumnar distance/Å | | |
| S ··· S | 3.73(1) | 3.663(3) |
| Se ··· S | 3.858(9) | 3.890(2) |
| The shortest intercolumnar distance/Å | | |
| Se ··· Se | 3.620(5)<br>3.639(5) | 3.670(1) |

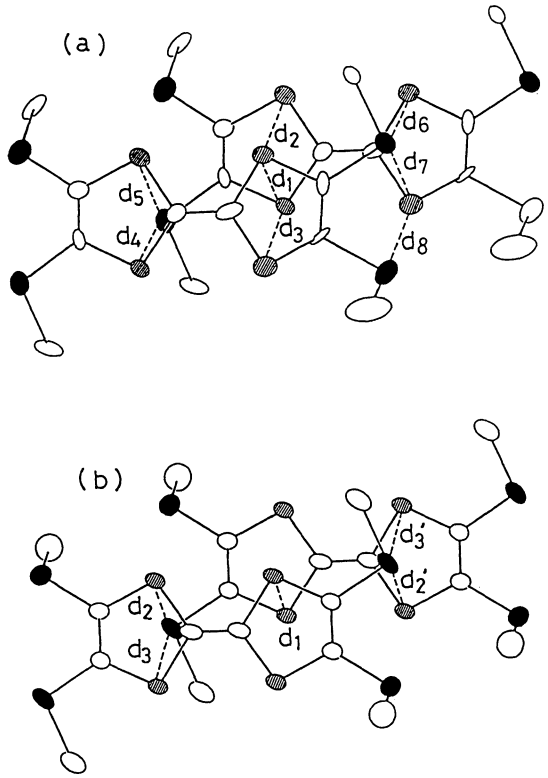


Fig. 2. Comparison of overlapping mode between the two phases.
(a) $TSeC_1$–TTF(L). Intracolumnar distances (<4Å): $d_1$(S1*···S3**)=3.73(1), $d_2$(S2*···S3**)=3.84(1), $d_3$(S1*···S4**)=3.85(1), $d_4$(Se1*···S1**)=3.856(8), $d_5$(Se1*···S2**)=3.997(8), $d_6$(S3*···Se3**)=3.885(8), $d_7$(S4*···Se3**)=3.964(9), $d_8$(S4*···Se4**)=3.952(9) Å.
Symmetry operations: *(*x*, *y*, *z*), **(*x*, 1+*y*, *z*).
(b) $TSeC_1$–TTF(H). Intracolumnar distances (<4 Å): $d_1$(S1*···S1***)=3.663(3), $d_2$(Se1*···S2**)=3.890(2), $d_3$(Se1*···S1**)=3.969(2) Å.
Symmetry operations: *(*x*, *y*, *z*), **(*x*, *y*, 1+*z*), ***(−*x*, −*y*, 2−*z*).

$C_6S_4Se_4$ skeletons is 3.568(4) Å and is nearly the same as that of $TSeC_1$–TTF(H) (3.570(1) Å). The densities of these two crystals are also nearly the same (Table 2).

Crystal structure of $TSeC_1$–TTF(L) is shown in Fig. 3. There exist intercolumnar short Se1 ··· Se3 contacts (3.620(5) and 3.639(5) Å), which are much shorter than the sum of the van der Waals radii (4.00 Å). These Se atoms form zigzag chains between neighboring columns along the stacking axis (Fig. 3(b)). These Se ··· Se chains are important to extend the molecular overlapping along the *b*-axis. However, these zigzag chains are formed by Se1 and Se3 atoms, and the other Se2 and Se4 atoms do not have strong intercolumnar interaction (only with the terminal methyl groups with the van der Waals contacts along the stacking axis). There are no short Se ··· Se contact along the *c*-axis. On the other hand, in the case of $TSeC_1$–TTF(H), short intercolumnar Se ··· Se contacts exist in nearly $a+b$ and $a-b$ directions (Fig. 4(b)). The H-phase has two-dimensional array of the short Se ··· Se contacts, whereas the L-phase has short Se ··· Se contacts only along one direction. It could be one of the reasons that melting point of $TSeC_1$–TTF(L) (92.5 °C) is lower than that of $TSeC_1$–TTF(H) (106.3 °C).

We tried to estimate the intermolecular overlap integrals to understand the cause of the difference of the electrical conductivities between these two phases. The overlap integrals calculated by the extended Hückel molecular orbitals between HOMOs for these two crystals are shown in Table 3. The overlap of $TSeC_1$–TTF(L) along the stacking axis (direction *s*) is a little larger than that of $TSeC_1$–TTF(H) (direction *s*). Moreover, in the $TSeC_1$–TTF(L) crystal, one molecule can have intermo-

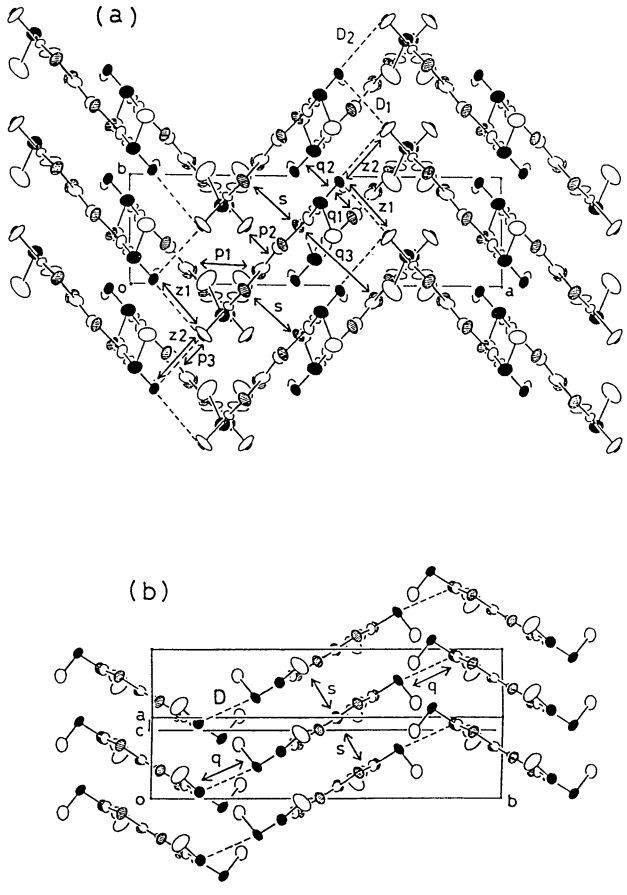


Fig. 3. Crystal structure of $TSeC_1$–TTF viewed nearly along the molecular short axis. The allows and the characters (s, p, q, z) indicate the directions of intermolecular interactions shown in Table 3.
(a) $TSeC_1$–TTF(L) (projected along the *c*-axis)
Dotted lines mean intercolumnar Se···Se distances: $D_1$=3.620(5), $D_2$=3.639(5)Å.
(b) $TSeC_1$–TTF(H)
Dotted lines mean intercolumnar Se···Se distances: $D$=3.670(1) Å.

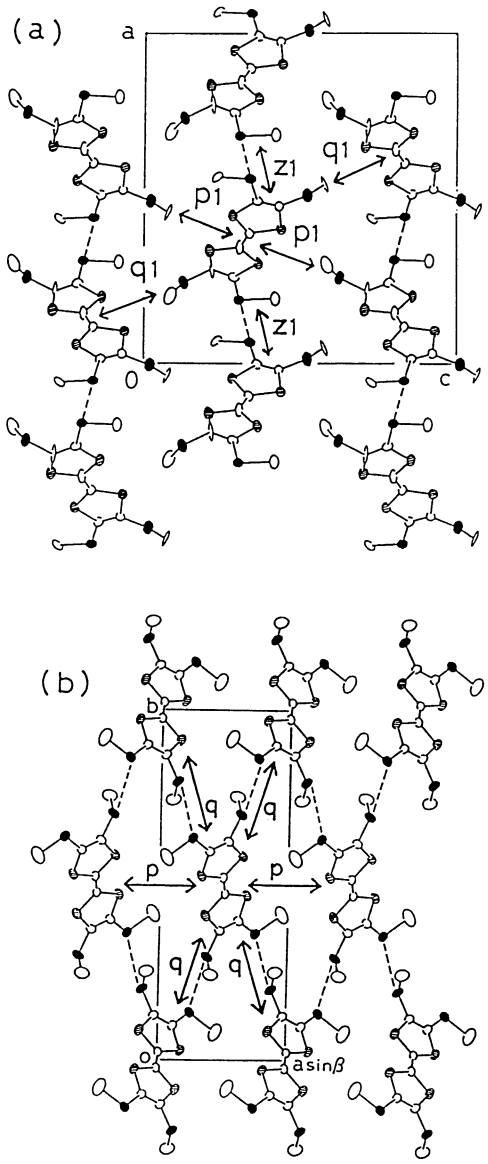


Fig. 4. Crystal structure of $TSeC_1$–TTF viewed nearly along the stacking axis. The arrows and the characters (p, q, s, z) mean the intermolecular interactions shown in Table 3.
(a) $TSeC_1$–TTF(L) (projected along the *b*-axis),
(b) $TSeC_1$–TTF(H) (projected along the *c*-axis).

Table 3. Overlap Integrals ($\times 10^3$) of the HOMOs for $TSeC_1$–TTF(L) and $TSeC_1$–TTF(H). (The symbols are directions of interactions shown in Figs. 3 and 4.)

| $TSeC_1$–TTF(L) | | $TSeC_1$–TTF(H) | |
|---|---|---|---|
| s | −3.69 | s | −3.20 |
| z1 | −0.107 | p | 0.371 |
| z2 | 0.00569 | q | −0.036 |
| p1 | −0.223 | | |
| p2 | 0.100 | | |
| p3 | 0.100 | | |
| q1 | 0.0765 | | |
| q2 | −0.0114 | | |
| q3 | −0.0114 | | |

lecular interactions with many neighboring molecules (Fig. 3(a) and (b)) and has larger overlap integrals in many directions than the case of $TSeC_1$–TTF(H). These facts are compatible with the result that the electrical resistivity and activation energy for conduction of $TSeC_1$–TTF(L) are lower than those of $TSeC_1$–TTF(H) (Table 2).

In summary, the $TSeC_1$–TTF(L) crystal has better overlap mode along the stacking axis and has larger intermolecular overlap integrals. This may be related to the low resistivity of the L-phase. On the contrary, these Se ··· Se contacts are only along the *b*-axis and do not form network like in $TSeC_1$–TTF(H). This two-dimensional Se ··· Se network may be associated with the higher melting point of the H-phase.

We thank Dr. T. Inabe (Institute for Molecular Science) and Professor T. Enoki (Tokyo Institute of Technology) for their valuable discussion.

**References**

1) H. Inokuchi, G. Saito, P. Wu, K. Seki, T. B. Tang, T. Mori, K. Imaeda, T. Enoki, Y. Higuchi, K. Inaka, and N. Yasuoka, *Chem. Lett.*, **1986**, 1263.

2) K. Imaeda, T. Enoki, Z. Shi, P. Wu, N. Okada, H. Yamochi, G. Saito, and H. Inokuchi, *Bull. Chem. Soc. Jpn.*, **60**, 3163 (1987).

3) H. Inokuchi, K. Imaeda, T. Enoki, T. Mori, Y. Maruyama, G. Saito, N. Okada, H. Yamochi, K. Seki, Y. Higuchi, and N. Yasuoka, *Nature*, **329**, 39 (1987).

4) H. Yamochi, N. Iwasawa, H. Urayama, and G. Saito, *Chem. Lett.*, **1987**, 2265.

5) P. Wang, T. Enoki, K. Imaeda, N. Iwasawa, H. Yamochi, H. Urayama, G. Saito, and H. Inokuchi, *J. Phys. Chem.*, **93**, 5947 (1989).

6) P. Wang, T. Inabe, C. Nakano, Y. Maruyama, H. Inokuchi, N. Iwasawa, and G. Saito, *Bull. Chem. Soc. Jpn.*, **62**, 2252 (1989).

7) "International Tables for X-Ray Crystallography," Kynoch Press, Birmingham (1974), Vol. IV.

8) T. Sakurai and K. Kobayashi, *Rep. Inst. Phys. Chem. Res.*, **55**, 69 (1979).

9) Tables of atomic parameters of H-atoms, anisotripic thermal parameters, and list of structure factors are deposited as Document No. 8973 at the Office of the Editor of Bull. Chem. Soc. Jpn.